Colloids and Surfaces B: Biointerfaces 217 (2022) 112691

Contents lists available at ScienceDirect

Colloids and Surfaces B: Biointerfaces

journal homepage: www.elsevier.com/locate/colsurfb

A photocrosslinking antibacterial decellularized matrix hydrogel with nanofiber for cutaneous wound healing

Fan Yu [a], Atta ur Rehman Khan [b], Hui Zheng [c], Xiaotong Li [a], Mohamed EL-Newehy [d], Hany EL-Hamshary [d], Yosry Morsi [e], Jun Li [f,*], Jinglei Wu [a,*], Xiumei Mo [a,*]

[a] State Key Laboratory for Modification of Chemical Fibers and Polymer Materials, Shanghai Engineering Research Center of Nano-Biomaterials and Regenerative Medicine, College of Biological Science and Medical Engineering, Donghua University, Songjiang, Shanghai 201600, China
[b] Department of Biotechnology, The University of Azad Jammu and Kashmir, Muzaffarabad, Pakistan
[c] Department of Thoracic Surgery, Shanghai Pulmonary Hospital, Tongji University School of Medicine, Shanghai, China
[d] Department of Chemistry, College of Science, King Saud University, P.O. Box 2455, Riyadh 11451, Saudi Arabia
[e] Faculty of Engineering and Industrial Sciences, Swinburne University of Technology, Boroondara, VIC 3122, Australia
[f] Department of Orthopedics, Shanghai Tenth People's Hospital, School of medicine, Tongji University, Shanghai 200072, China

ARTICLE INFO

Keywords:
Decellularized matrix
Photocrosslinking hydrogel
Wound healing
Multifunction
Nanofiber

ABSTRACT

ddECMMA is the methacrylating product of decellularized dermal extracellular matrix with biological signals and capable of photocrosslinking. Thiolated chitosan (TCS) is an effective antibacterial component. PCLPBA is a kind of plasma-treated polycaprolactone nanofiber dispersions (PCLP) that regulates macrophage polarization and promotes angiogenesis. In this study, we obtained ddECMMA via methacrylation reaction. TCS was prepared by reaction between chitosan and thioglycolic acid. PCLPBA was fabricated via reaction between PCLP and 3-buten-1-amine. TCS and PCLPBA were mixed in ddECMMA solution and photocrosslinked to form DTP4 hydrogel. The hydrogel showed rapid gelation, good mechanical strength, antibacterial and antioxidant properties. When it was cocultured with NIH 3T3 cells, the cells showed good morphology and proliferation rate. After applying it to the full-thickness cutaneous wound, wounds almost healed in 2 weeks via re-epithelialization and neovascularization with negligible scar tissue. The results indicate that DTP4 hydrogel is a promising candidate for clinic skin wound healing.

1. Introduction

Injectable hydrogels are appealing for tissue therapy since the easy integration of cells or bioactive drugs [1–3], uncomplicated operation [4], simplicity of gel formation by irradiation [5] and high cell viability [6]. Numerous biomaterials have been developed for in-situ gelation hydrogels, which mimic the composition and structural cues of native extracellular matrix (ECM) [5,7]. In comparison, the present established hydrogels are insufficient to replicate the complex functions in tissues, such as the ultra-structure of ECM, chemical composition and antibacterial property.

Recently, decellularized extracellular matrix (dECM), which originated from living tissues, has become famous in tissue regeneration [8,9]. Due to the inherent ultrastructure, bioactive molecular and chemical composition, dECM can impact cell proliferation, migration and differentiation [10–12]. Extensive studies have reported dECM-based scaffolds, which showed excellent effect in cartilage [13], heart [14], tendon [15] and skin [16]. However, the gelation of dECM hydrogel takes 60 min at room temperature with weak mechanical strength [17]. Thioglycolic acid has been reported to enhance the antibacterial ability of materials, including silver nanoparticles [18], CdSe aquantum dots [19] and chitosan [20]. Thioglycolic acid modified chitosan (TCS) shows outstanding antibacterial activity against Gram-positive bacteria, Gram-negative bacteria and fungi than chitosan

Abbreviations: ECM, extracellular matrix; dECM, decellularized extracellular matrix; TCS, Thioglycolic acid modified chitosan; ddECMMA, methacrylating decellularized dermal extracellular matrix; PCLPBA, 3-buten-1-amine modified polycaprolactone nanofiber with plasma treatment; UV, Ultraviolet; PEGDA, poly (ethylene glycol) diacrylate; CCK-8, Cell Counting Kit-8; *E. coli*, *Escherichia coli*; *S. aureus*, *Staphylococcus aureus*; DPPH, 1,1-Diphenyl-2-picrylhydrazine; AA, Ascorbic acid.

* Corresponding authors.
E-mail addresses: lijunspine@163.com (J. Li), jw@dhu.edu.cn (J. Wu), xmm@dhu.edu.cn (X. Mo).

https://doi.org/10.1016/j.colsurfb.2022.112691
Received 22 April 2022; Received in revised form 20 June 2022; Accepted 4 July 2022
Available online 8 July 2022

[21]. Besides, it has negligible cytotoxicity [22]. Nanofiber composite hydrogel has been used as a promising scaffold due to its similarity in microstructure [23]. Studies indicate that nanofiber composite hydrogel can regulate macrophage polarization and promote angiogenesis [24, 25].

In this study, we developed a multifunctional decellularized matrix hydrogel with antibacterial, antioxidant properties and nanostructure, which could satisfy all the scaffold requirement of rapid gelation, antibacterial property and ultrastructure for scaffold. The composite hydrogel is composed of ddECMMA, TCS and 3-buten-1-amine (BA) modified polycaprolactone nanofiber with plasma treatment (PCLPBA). To increase the stiffness of hydrogel, poly (ethylene glycol) diacrylate (PEGDA) was added at a concentration of 3 wt%. Ultraviolet (UV) light was used for rapid crosslinking of hydrogels. The properties of hydrogels were systematically characterized. The efficacy of hydrogels was also estimated in full-thickness wound model.

2. Materials and methods

2.1. Materials

Chitosan (95 % deacetylation) and polycaprolactone (Mw ≈ 80 kDa) were purchased from Sigma-Aldrich, 3-buten-1-amine (BA) and methacrylic anhydride were purchased from Sun Chemical technology (Shanghai). PEGDA (Poly(ethylene glycol) diacrylate) was purchased from TCI Shanghai Co., Ltd. Pepsin (purity of 99 %, 1: 15,000 U), DMEM (Dulbecco's modified eagle medium), PBS (Phosphate Buffered Saline), Live & Dead staining assay and Cell Counting Kit-8 (CCK-8) assay were obtained from Beijing Solarbio Science & Technology Co., Ltd. Serum and antibiotics were purchased from Thermo Fisher Scientific Inc. DNA extraction kits were provided by Tiangen Biochemical Technology Co., Ltd. All other chemical reagents were purchased from Shanghai Macklin Biochemical Co., Ltd. All reagents were analytic quality and used as received.

2.2. Extraction of ddECM from Swine dermis tissue and residual DNA test

Full-thickness skin was purchased from mature male pigs (6 months old, weight above 100 kg) in the Longyuan market (Songjiang district). The decellularization and solubilization processes (Fig. 1B) were conducted from a previous study [26]. Briefly, after removing subcutaneous fat tissue and hair, the skin was sliced into pieces with a thickness of 2–3 mm and length of 3 cm. 50 g of skin slice was stirred in 200 ml 0.25 % trypsin for 6 h and washed for 15 min with ultrapure water 3 times. The processed skin was agitated in 200 ml 70 % ethanol for 10 h, then 200 ml 3 % hydrogen peroxide for 15 min and 30 min wash in ultrapure water, respectively. The skin sample was processed with the following solutions sequentially: 500 ml 1 % Triton X-100 (to lyse the cell wall) with 0.26 % EDTA and 0.69 % Tris for 6 h, then a replaced 500 ml solution for another 16 h and 15 min wash with 500 ml ultrapure water for 3 times. The skin sample was stirred in 500 ml 0.1 % peracetic acid (to inactivate the virus) with 4 % ethanol for 2 h, 15 min wash with 500 ml PBS for 2 times and 15 min wash with ultrapure water for 2 times, respectively. The sample was frozen at - 80 °C overnight, lyophilized for 3 days and then powered at 12,000 rpm for 5 min 6 times sequentially. After sterilization with ethylene oxide, ddECM was obtained and kept at - 80 ℃ until use.

For DNA extraction, 20 mg samples of ddECM and fresh dermal tissue were cut into pieces and put in different tubes. Then 1 ml PBS was added, followed by homogenization for 5 min. Then DNA solution was extracted with Tiangen Kit. For DNA concentration detection, NanoDrop (Thermo Scientific) was used. The type of substance was set as DNA, then 1.5 μL DNA solution was added to determine its concentration, and values at 260/280 and 260/230 were recorded to measure the DNA concentration.

Agarose gel electrophoresis detection was processed as follows. DNA sample of fresh dermal tissue was diluted by 30 times. Then 3 μL DNA samples were loaded to the spotting hole, respectively. The agarose gel was processed for 20 min under 200 V and then placed in an imaging analysis system.

2.3. Preparation of ddECMMA, TCS and PCLPBA nanofiber

The preparation of ddECMMA was carried out from a previous study [27]. Briefly, ddECM was digested with pepsin (1 mg/ml) in hydrochloric acid (0.01 M HCl) solution. The solution was under constant stirring at 300 rpm overnight. The pH was adjusted to 9.0 and kept for 1 h to inactive the pepsin. Then it was adjusted to 7.5 before methacrylic anhydride was added dropwise at a concentration of 2.5 ml/g. The solution was stirred for 12 h, followed by dialysis with distilled water for 4 days. The water was changed 3 times a day. The ddECMMA was obtained after lyophilization.

The synthesis of TCS and preparation of PCLPBA were conducted from previous studies [23,28]. For TCS synthesis, 0.5 g chitosan was dissolved in HCl (0.09 M, 50 ml), followed by EDC (1.2 g) and 0.38 ml thioglycolic acid being added sequentially. Then 0.5 M NaOH was added to adjust the pH to 5.0. After stirring for 5 h and dialysis for 3 days, TCS was obtained after freeze-drying. TCS was then homogenized and kept at 4 ℃.

For the fabrication of PCLPBA (Fig. 1A), 1.6 g PCL was dissolved in 10 ml dichloromethane and dimethylformamide (9/1, v/v). Then electrospinning was applied at the ratio of 2 ml/h and 20 KV voltage. Nanofiber was cut into 1 × 3 cm pieces, homogenized at 12,000 rpm for 30 min and plasma-treated for 5 min to fabricate PCLP (plasma treated polycaprolactone nanofiber). Then 10 g PCLP nanofiber was dispersed in 50 ml DI water with 2.3 g EDC and 1.38 g NHS added. Then 0.63 g 3-buten-1-amine (BA) was added and stirred for 12 h. The nanofiber was then washed with DI water and alcohol for 3 times, respectively. After freeze-drying, the PCLPBA was obtained and kept at 4 ℃.

2.4. Preparation of hydrogels

The hydrogels precursor solution was prepared according to Table. S1. The process was conducted as Fig. 1C showed. Briefly, ddECMMA was dissolved in LAP solution (0.1 wt %). Then the TCS, PEGDA and PCLPBA were added at varied ratios and stirred for 3 h. Hydrogels were prepared after UV irradiation for 100 s (100 mW/cm^2).

2.5. Characterization

2.5.1. Fourier transform infrared spectra (FT-IR) and Nuclear magnetic resonance spectroscopy (^{1}H NMR) analysis

FT-IR was performed with a Nicolet 6700 spectrometer in transmission mode. ^{1}H NMR was conducted on a Bruker Avance 600 NMR spectrometer. The solvent of ddECMMA for NMR testing was deuterium oxide (D_2O).

2.5.2. Rheological test

The rheological tests were performed using a Thermo Fisher rotational rheometer (HAAKE MARS 60 Rheometer) with UV light components. 20 mm parallel plates were used with a 0.2 cm distance between plates. Angular velocity ω was 10 rad/s, and dynamic time scan γ_0 was 1 % during UV light irradiation. The samples were loaded at 37 °C for 50 s for the dynamic modulus test, followed by UV light irradiation for 100 s. Then UV light irradiation stopped with dynamic modulus continuing to measure change for another 90 s

2.5.3. Morphology of hydrogels

Freshly prepared hydrogels were frozen at − 80 °C for 12 h. Then hydrogels were lyophilized for three days, before samples were gold sprayed with 10 nm thick platinum (6 mA, 45 s). SEM images were taken using a scanning electron microscope (Phenom XL).

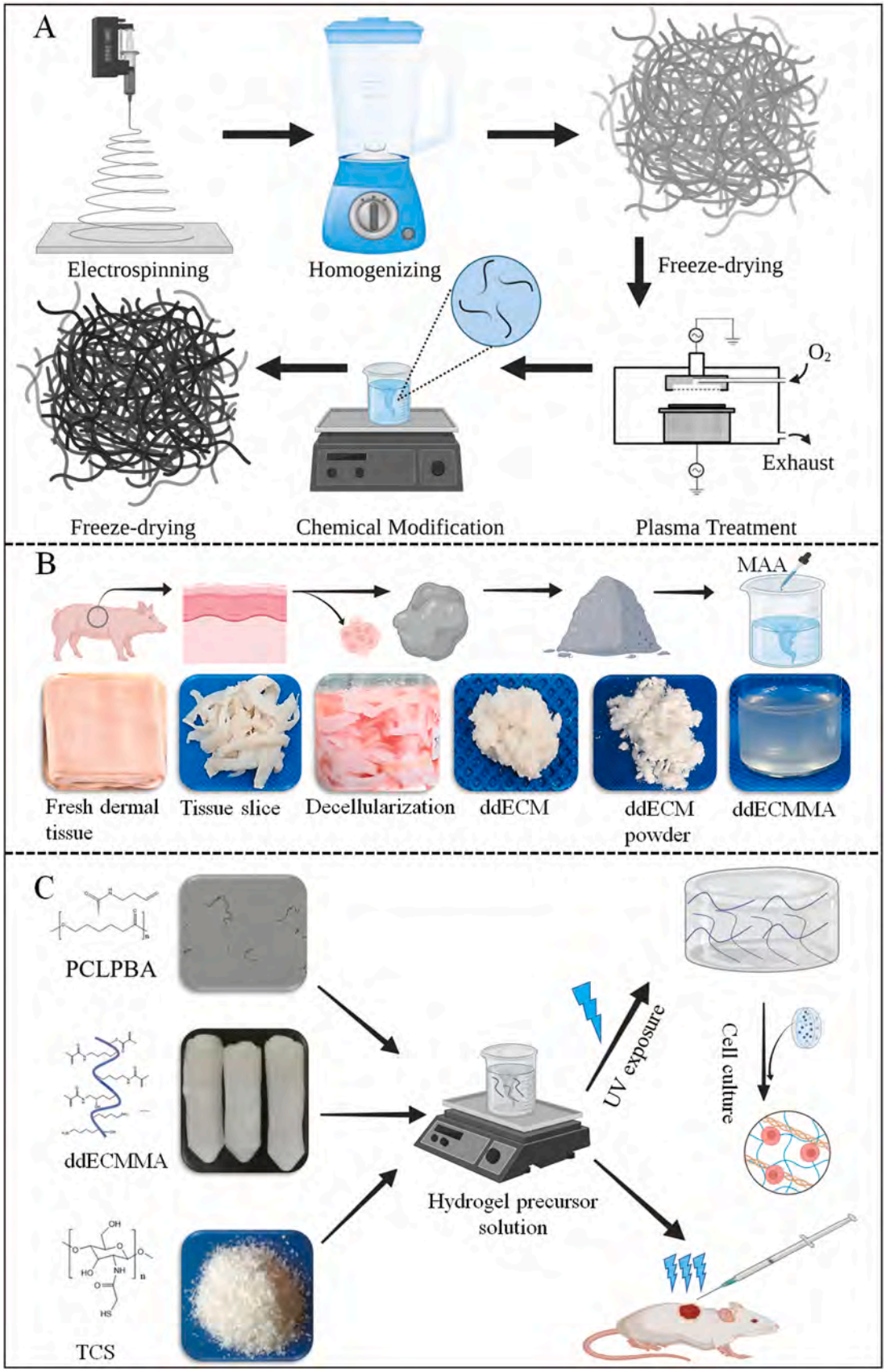

Fig. 1. Schematic image of PCLPBA preparation, decellularization and hydrogels fabrication. (A) The preparation of PCLPBA. PCL was fabricated into nanofiber, then homogenized into dispersions. After plasma treatment, chemical modification and freeze-drying, PCLPBA was obtained. (B) Decellularization and the synthesis of ddECMMA, (C) Schematic image of DTP hydrogel fabrication.

2.5.4. Swelling ratio

The swelling ratio of hydrogels was carried out by the gravimetric method [29]. Hydrogels were soaked in PBS overnight to reach the swelling equilibrium and weighted as w_s. Moreover, hydrogels were freeze-drying for 24 h and weighed as w_d. The following equation calculated the swelling ratio of hydrogel:

$$Swelling\ ratio = \frac{w_s - w_d}{w_d}$$

2.5.5. Degradation test

PBS containing collagenase (1 mg/ml) was used as degradation solutions for the experiment. The hydrogel was weighed after photocrosslinking and recorded as w_0. Subsequently, they were transferred to containers with 15 ml solution. The solution was changed once a day. Hydrogels were placed in an incubator at 37 °C, taken out from the solution at given time points, removed from surface moisture, weighed and recorded as w_1. Three independent samples were tested for each timepoint. The percentage of residual hydrogel mass was calculated as follows:

$$Weight\ remaining\ ratio = \frac{w_1}{w_0} \times 100\%$$

2.5.6. Mechanical property test

Hydrogels were placed in PBS for 2 h before the mechanical property test. The hydrogels were prepared into Ø 10 mm × 6 mm size cylinders, then placed between two parallel metals and characterized under uniaxial compression (HY-940FS; Shanghai Hengyu Instrument). Hydrogel cylinders were compressed in 5 mm/min. Each group tested five independent samples. The Young's modulus of hydrogels was calculated by the curve corresponding to 0–20 % strain.

2.5.7. Antibacterial test

Escherichia coli (*E. coli*) and *Staphylococcus aureus* (*S. aureus*) were used as representative Gram-negative and positive bacteria, respectively. Sterilized MHB broth was prepared. The bacteria were added to the broth and incubated overnight at 37 °C. The sterile hydrogel was formed in 24-well plates with UV irradiation. Subsequently, 10 μL of bacterial suspension was added to the surface, 1 ml of the liquid medium was added to the experimental group. After incubation at 37 ℃ for 18 h, the colony formed on the agar plates of Petri dishes.

2.5.8. Antioxidant test

The antioxidant test was conducted according to the previous report [30]. 1,1-Diphenyl-2-picrylhydrazine (DPPH) assay was dissolved in ethanol with a concentration of 0.3 mM. Hydrogels (Ø 10 mm × 4 mm) were added into tubes with 5 ml DPPH solution and kept in dark for 30 min. Ascorbic acid (AA) was mixed with 5 ml DPPH solution as the standard group. DPPH solution was chosen as a blank group. The following equation calculated the antioxidant activity:

$$Antioxidant\ activity = \frac{OD_B - OD_H}{OD_B} \times 100\%$$

OD_B is the absorption of the blank group. OD_H is the absorption of hydrogels. Images were taken after 30 min.

2.5.9. Cell experiment

The sterilized hydrogels were prepared on a 48-well plate. Then NIH 3T3 cell suspensions were prepared at a density of 40k cell/ml. The cells were planted on hydrogels with 20 k cell/ well. The cells were cultured in an incubator (37 °C, 5 % CO_2). On days 1, 3 and 5, CCK-8 assay and Live & Dead staining kit were used for cytotoxicity testing and fluorescence photographs.

2.5.10. Animal experiment

All relevant animal experiments comply with the ARRIVE guidelines and carried out in accordance with EU Directive 2010/63/EU for animal experiments. Also, these were approved by the Animal Ethics Committee of Tongji University (SHDSYY-2021–4427). Mature male SD rats were anaesthetized with inhaled isoflurane, followed by the back hair completely shaved. Then a full thickness skin defect was established with a diameter of 15 mm by surgical instruments. The wound SD mice were randomly divided into 4 groups: the DTP4 group, DTP0 group, DP group and Blank group. For the control group, the skin defect was not treated. Every hydrogel tested three independent samples. Hydrogel precursor solutions were injected into the wound defects (Fig. 1C and Video. S1) and irradiated for gelation (100 mW/cm^2, 100 s). Experimental animals were executed at 1, 2 and 3 weeks postoperatively. The wound images were taken subsequently. The wound closure ratio was calculated using ImageJ (NIH) software using the following formula.

Supplementary material related to this article can be found online at doi:10.1016/j.colsurfb.2022.112691.

S_0 was the initial wound area, and S_1 was the wound area at different time points. The traumatic tissue was then excised and immediately immersed in 4 % paraformaldehyde for 10 h and stored at 4 °C until further analysis.

Histological staining was performed at 1, 2 and 3 weeks. The wound and surrounding tissue were resected, rinsed with PBS, fixed in 4 % paraformaldehyde, and then immersed in paraffin. 5 μm sections of skin tissue were cut, dehydrated and stained with hematoxylin-eosin (H&E). Also, tissues were stained with Masson's trichrome.

Immunohistochemical staining of CD31 was performed at 1, 2 and 3 weeks. For antigen recovery, the deparaffinized and rehydrated tissue area were incubated with citric acid (pH = 6.0) solution in a microwave oven followed by cooling to room temperature and rinsing in 0.01 M PBS for 5 min. To block endogenous peroxidase and serum, slides were sequentially treated with 3 % H_2O_2 for 25 min and 3 % bovine serum albumin for 30 min. The primary antibody, CD31 primary antibody, was incubated at 4 °C overnight. The biotinylated goat antirabbit (1:200) was then added and incubated for 30 min. The slides were incubated with 3,3′-Diaminobenzidine tetrahydrochloride and H_2O_2 solution for visualization. Slides were counterstained with hematoxylin for 1 min, followed by dehydration in sequential ethanol before sealing. All slides were viewed with a CIC XSP-C204 fluorescence microscope.

2.6. Statistical Analysis

Comparative analysis of data was performed using Origin 2018, and results were expressed as mean ± standard deviation. Significant differences were obtained using the one-way ANOVA, Turkey test, which considered *$p < 0.05$ as statistically significant differences between samples.

3. Results

3.1. Dermal decellularization

Fig. 2A showed that the colour of tissue sample changed from yellow to white after decellularization. The DNA concentration was reduced from 364.8 to 12.7 ng/mg, showing statistically significant difference between dermal tissue and ddECM ($p < 0.05$). The agarose gel electrophoresis results (Fig. 2B) showed that the decellularization process substantially affects the integrity of DNA, leading to its decomposition. Compared with marker bands, no evident bands were seen in the ddECM group (lane 1 and 2). In contrast, clear bands over 10,000 bp (base pair) were observed in the fresh dermal tissue group (lane 3 and 4) even after its DNA sample was diluted by 30 times.

The H&E staining of ddECM (Fig. 2E) showed matrix (pink) without obvious nuclear dots from fresh native tissue (Fig. 2C). The absence of nuclei of ddECM was confirmed in the Masson's staining images (Fig. 2F), while the native tissue showed many purple-brown dots (Fig. 2D). The results indicated that the decellularization significantly

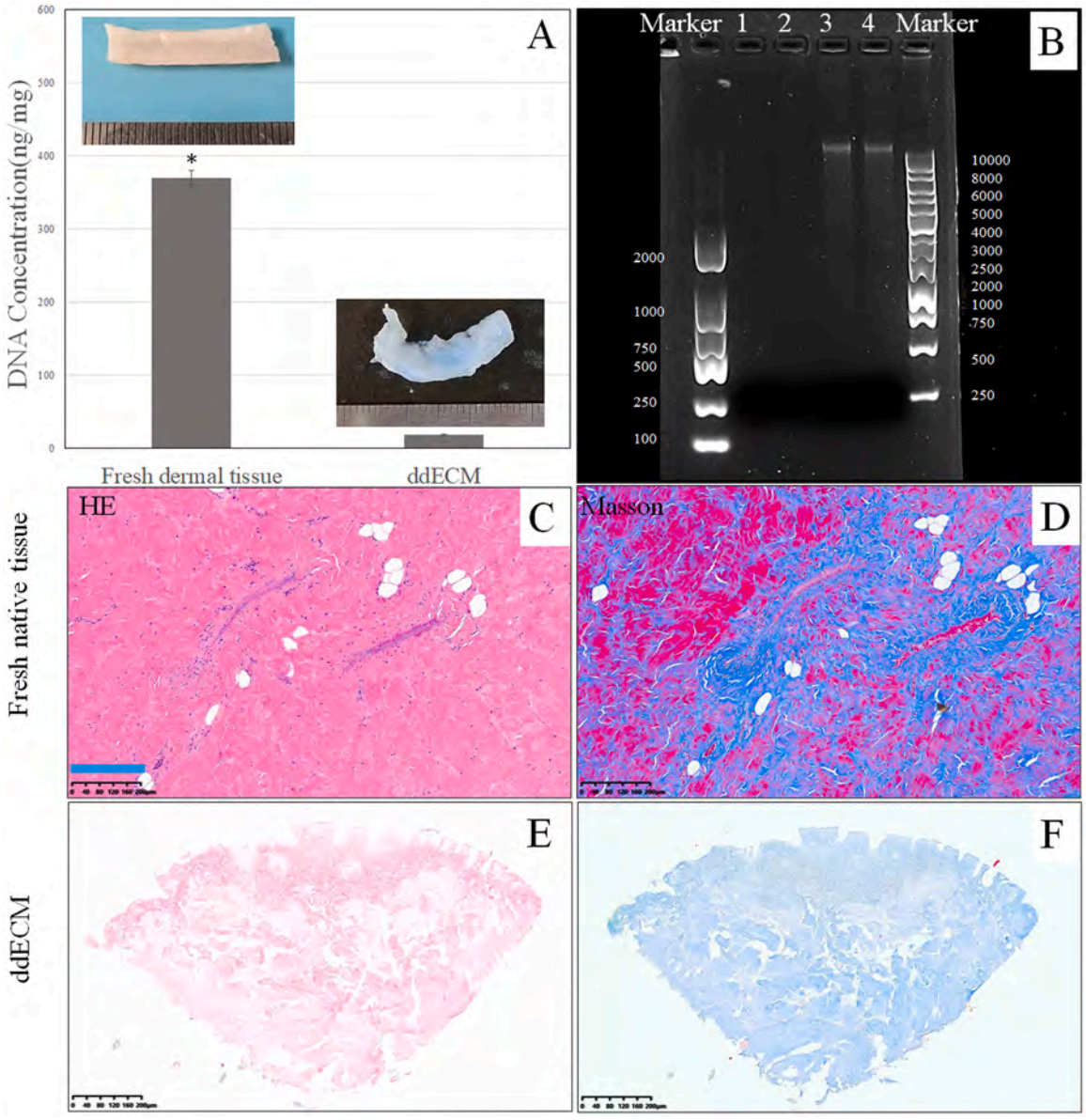

Fig. 2. Images representing the confirmation of decellularization. (A) Quantification of DNA contents in fresh dermal tissue and ddECM. Each group tested three independent samples. (B) Probing DNA with agarose gel electrophoresis. Lane 1 and 2 represented ddECM. Lane 3 and 4 represented fresh dermal tissue. (C, D) H&E and Masson's staining of fresh native dermal tissue, respectively. (E, F) H&E and Masson's staining of ddECM, respectively. The scale bar is 200 μm.

reduced DNA content.

3.2. FT-IR and ^{1}H NMR characterization

The natural protein in ddECM contains a lot of secondary structure in the amide I band (1600–1700 cm^{-1}), such as α-helix, β-sheet and random coil structure [31,32]. Fig. 3A showed that the characteristic peaks for ddECM were 1628 and 1546 cm^{-1}, which belonged to amide I and amide II, respectively. After reaction, the peaks of ddECMMA shifted to 1606, 1414, and 1031 cm^{-1}, corresponding to C═O stretching (amide I), N-H bending (amide II) and C-N stretching, and N-H bending (amide III), respectively. The methacrylation was further confirmed by ^{1}H NMR spectrometry. Fig. 3B exhibited the ^{1}H NMR spectra of ddECM and ddECMMA. New peaks at 5.7 and 6.1 ppm were observed at ddECMMA spectra, corresponding to the acrylic proton. The results confirmed the preparation of ddECMMA.

The preparation of PCLPBA and TCS were confirmed by ^{1}H NMR spectrometry. New peaks appeared in PCLPBA spectra at 5.2 ppm (Fig. S1), which were the peaks of BA. New peaks were observed in TCS spectra at 1.1 ppm (Fig. S2), which were the absorption peaks of thiol group. The change of peak intensity at 2.0 ppm indicated that thioglycolic acid reacted with amino group of chitosan. These results confirmed the preparation of PCLPBA and TCS.

3.3. Hydrogel formation and morphological study

Fig. 3C showed the optical and SEM images of hydrogels. Hydrogels turned from transparent to opaque with composition changes. PCLPBA evenly dispersed in DTP0 and DTP4 hydrogels. All hydrogels showed interconnected porous structure. The pore size became smaller with TCS, due to denser network (Fig. S3). Besides, the gelation could finish within 60 s (Fig. S4).

3.4. Mechanical and rheological properties of the hydrogels

Fig. 4A showed that all hydrogels exhibited a strain of more than 40

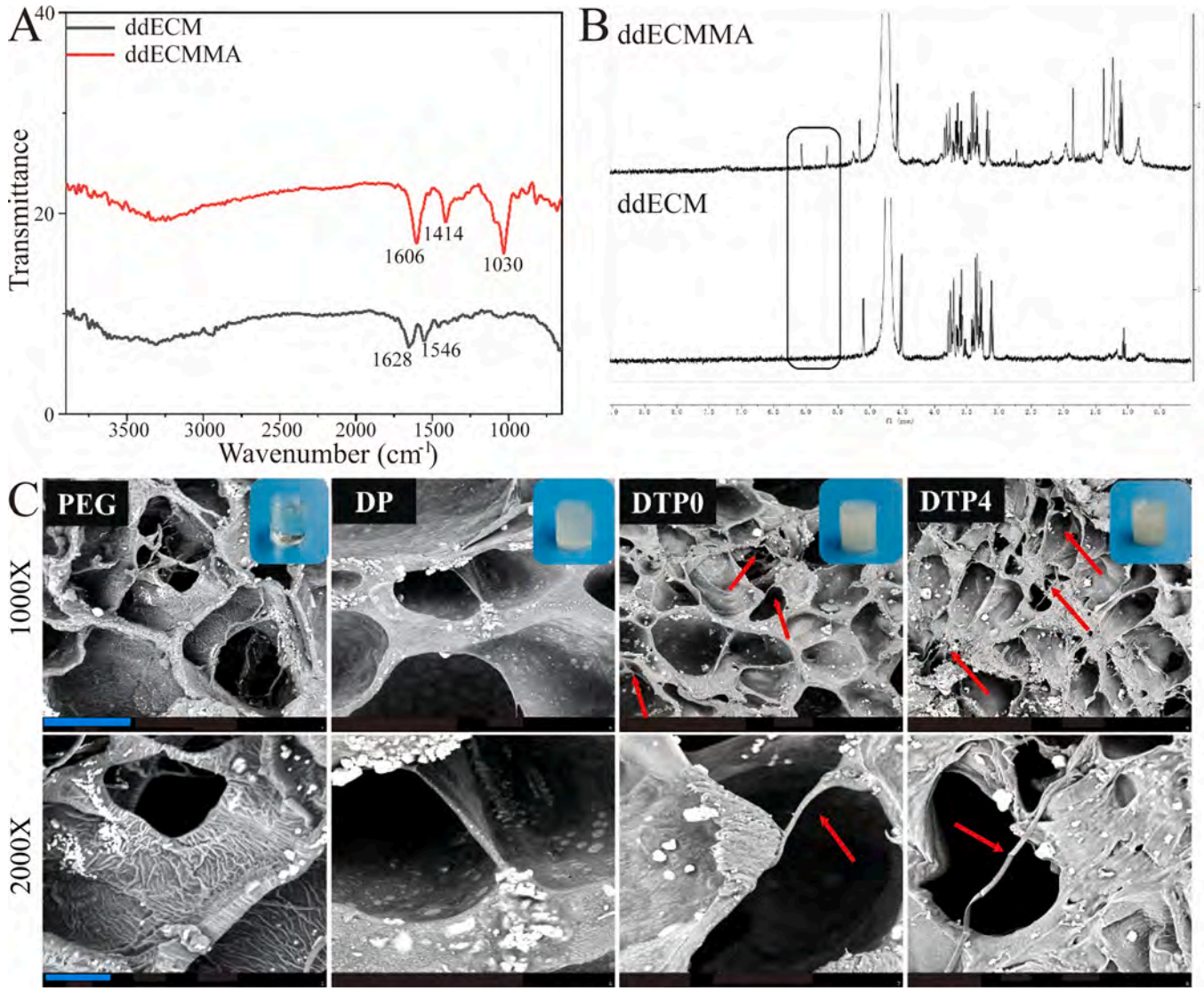

Fig. 3. Physicochemical characterization of hydrogels. (A) FT-IR spectra of ddECM and ddECMMA, (B) ^{1}H NMR spectra of ddECM and ddECMMA, (C) SEM images of lyophilized hydrogels. The magnifications are 1000X and 2000X. Red arrow showing the PCLPBA nanofiber. Scale bars are 80 μm and 20 μm, respectively. (For interpretation of the references to colour in this figure, the reader is referred to the web version of this article.)

% without breakage. The compression strength of DTP4 had been significantly improved. The DTP4 hydrogel didn't break, even at a stress of 0.42 MPa and a strain of 78.5 %. Furthermore, DTP4 hydrogel showed improved compression strength and Young's modulus that increased from 360.4 KPa to 419.6 KPa (Fig. 4C) and from 33.8 KPa to 41.5 KPa (Fig. 4B), respectively. Fig. 4D showed that all hydrogels had swelling ratios of more than 12. DTP4 had a higher swelling ratio (14.4 ± 0.4) than other hydrogels. There was no statistical difference between DTP4 and other hydrogels. The swelling ratio ranked in order of PEG < DP < DTP0 < DTP4.

UV irradiation was employed to determine the rheological properties. Fig. 4F and Fig. 4G showed the storage modulus (G′) and loss modulus (G") of hydrogels, respectively. G′ and G" remained unchanged in the first 50 s. Later, a sharp increase in G′ and G" was observed from 50 to 150 s with UV irradiation, indicating the gelation of hydrogel. G′ and G" kept increasing from 150 to 240 s Fig. 4H showed G′ values at 240 s, with significant differences observed between each two groups. The G′ of PEG, DP, DTP0 and DTP4 were 1831.6 Pa, 2287.1 Pa, 3366.3 Pa and 4069.3 Pa, respectively. Fig. 4I showed G" values at 240 s. No significant difference was found between PEG and DP group, while significant differences were observed between other groups. The G" of PEG, DP, DTP0 and DTP4 were 16.4 Pa, 18.0 Pa, 26.9 Pa and 37.8 Pa, respectively.

3.5. *In vitro degradation test*

A suitable degradation ratio is important for scaffold. The *in vitro* degradation properties of hydrogels were characterized with using collagenase in PBS (Fig. 4E). Hydrogels exhibited moderate degradation with time except PEG, which showed the least degradation. After 48 h, the residual mass for PEG, DP, DTP0, and DTP4 remained 97.1 %, 0 %, 0 % and 56.3 %, respectively. ddECMMA increased the degradation ratio of DP. PCLPBA also increased the degradation ratio of DTP0 due to intake of collagenase. However, the addition of TCS decreased the degradation ratio of DTP4 due to high network density. Results indicated that all hydrogels were biodegradable.

3.6. *Antioxidant Activity*

Fig. 5C exhibited the antioxidant activity of hydrogels. The colour of DTP4 and AA changed from purple to yellow due to radical scavenging. In contrast, other hydrogels showed negligible color changes. The

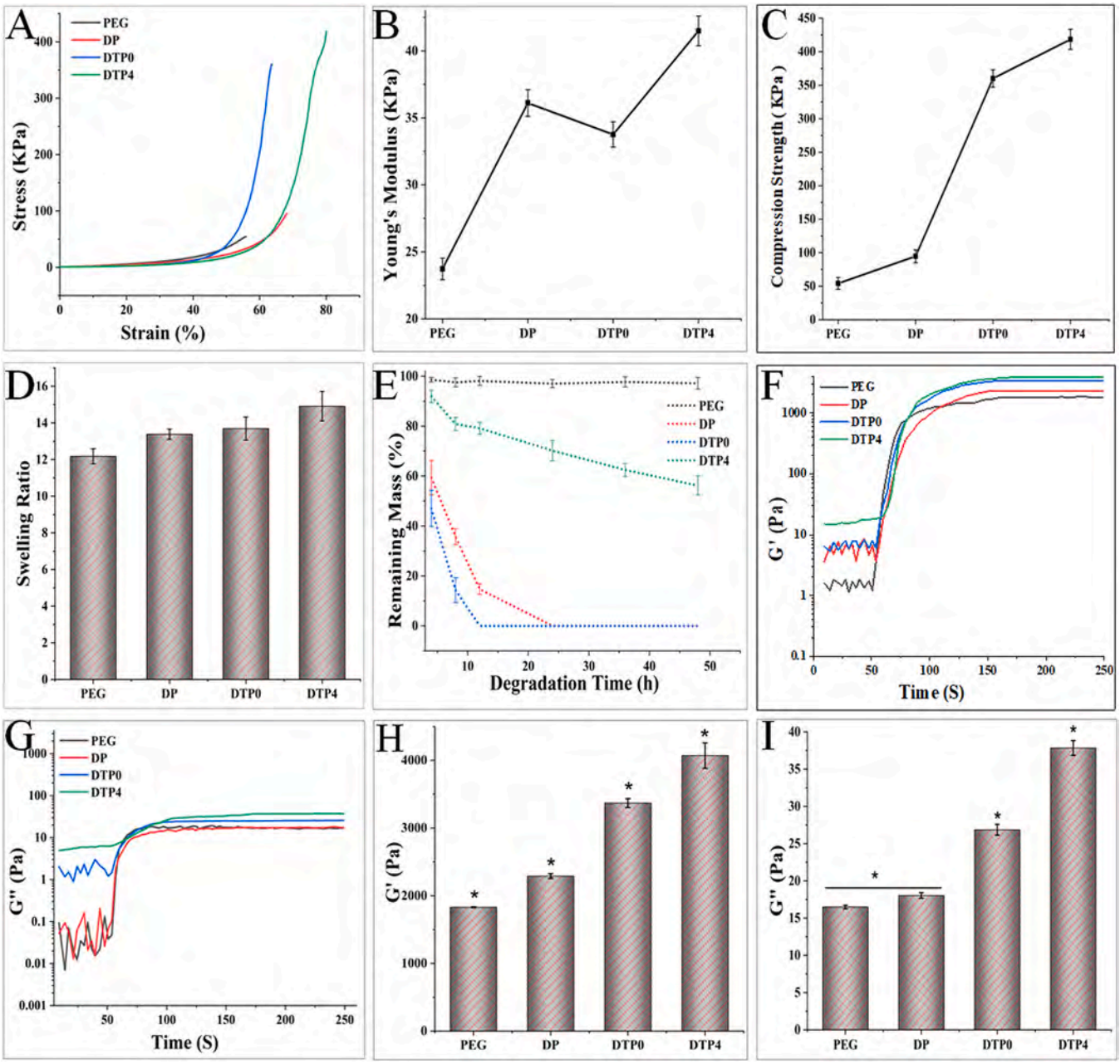

Fig. 4. Mechanical and rheological properties of the hydrogel. (A) Typical stress-strain curve, (B) Young's modulus, (C) Compression strength, (D) Swelling ratio, (E) Degradation graph, (F) The storage modulus (G'), (G)The loss modulus (G''), (H) Statistical analysis of G', (I) Statistical analysis of G''. Each group tested three independent samples.

antioxidant activities of PEG, DP, DTP0 and DTP4 hydrogel remained 12.2 %, 31.7 %, 27.9 % and 90.4 %, respectively. The results indicated that TCS was the main factor in bringing antioxidant potential.

3.7. Biological evaluation

3.7.1. In vitro cell culture

The viability of NIH 3T3 was assessed through CCK-8 assay and Live & Dead staining. Fig. 5A and Fig. 5B exhibited the CCK-8 and Live & Dead staining results, respectively. According to Fig. 5A, cell proliferate well on all hydrogels. On day 3, there was no significant difference between PEG and DP, while DTP0 and DTP4 showed significant differences with these two hydrogels. On day 5, significant differences were observed among all hydrogels. The OD (optical density) values of hydrogels were arranged in following order: PEG < DP < DTP0 < DTP4. The result indicated that ddECMMA and TCS promoted cell proliferation effectively. Cell viabilities were also measured. During 5 days' culture, all hydrogels showed excellent cell viabilities above 90 % and no significant difference were observed (Fig. S6). Live & Dead staining showed that NIH 3T3 cells represented a spherical morphology on hydrogels at Day 1(Fig. S7). At Day 3 & Day 5, scattered cells were visible on PEG hydrogel, while more cells were observed on other hydrogels (Fig. 5B). Besides, cells represented a spherical morphology on PEG hydrogel, whereas cells spread well on other hydrogels. Overall results indicated that DP, DTP0 and DTP4 promoted cellular proliferation hence could be considered biocompatible and nontoxic.

3.7.2. Antibacterial properties

S. aureus and *E. coli* were selected to assess the antibacterial property of hydrogels. Fig. 5D showed the bacterial colonies density on various

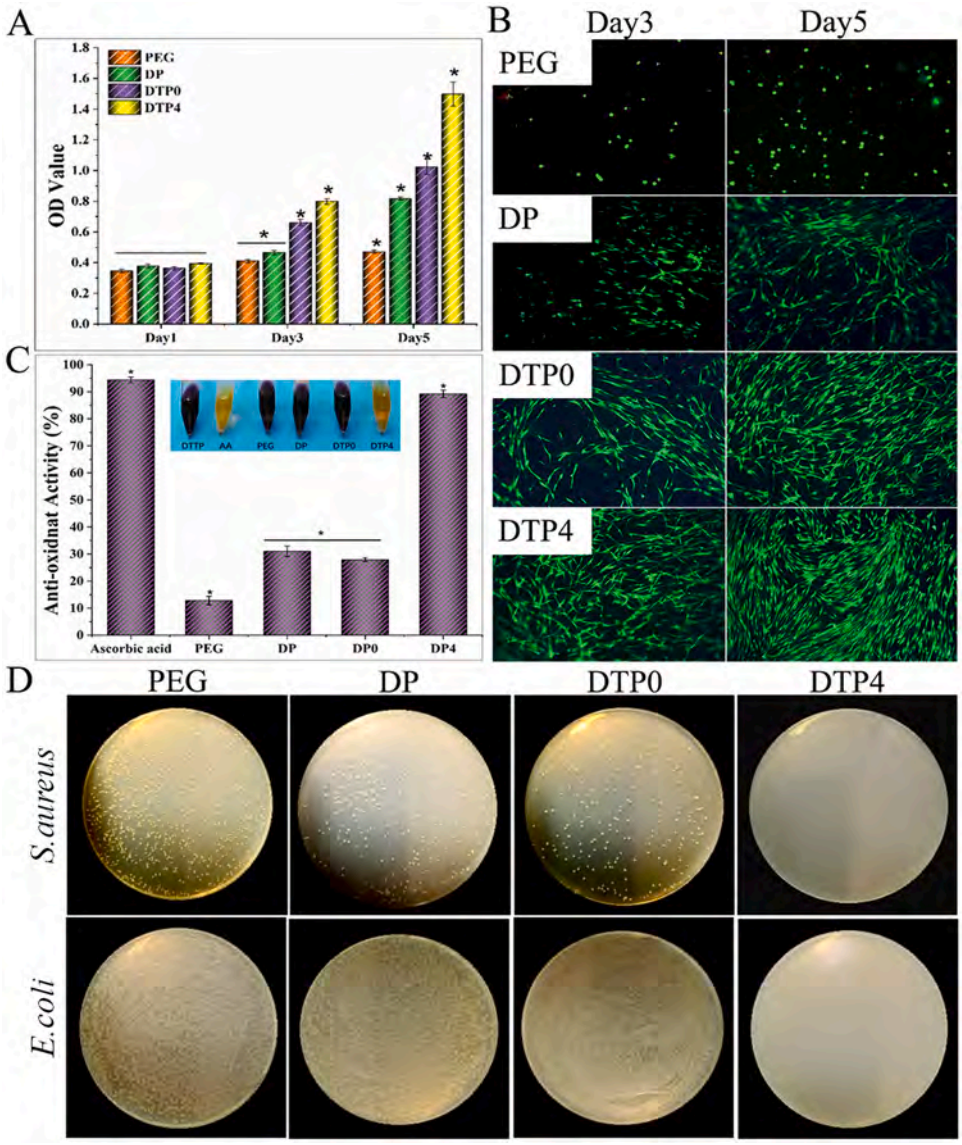

Fig. 5. Representative figure of *in vitro* biological evaluation of hydrogels. (A) CCK-8 results of NIH 3T3 cell on hydrogels, (B) Live & Dead staining of NIH 3T3 cells, (C) Antioxidant activity of various hydrogels. AA represented ascorbic acid, (D) Bacterial colonies on culture plates after being treated with various hydrogels. Scale bar is 100 μm. Each group tested three independent samples. Concentrations of *S.aureus* and *E.coli* for culture plate are 1.0×10^6 CFU/ml and1.0×10^7 CFU/ml, respectively.

plates. PEG, DP and DTP0 groups showed no obvious effect on both bacterial strains, while DTP4 showed drastically diminished bacterial, indicating that DTP4 possessed excellent antibacterial activity. And it was further proved by the bacteria colonies on agar plates (Fig. S5). Furthermore, SEM images of bacteria on hydrogels showed that both *S. aureus and E. coli* was inhabited on DTP4 hydrogel with colonies decreased (Fig. S8). Besides, bacteria shrinked and were encapsulated by hydrogel. The results indicated that DTP4 hydrogel is an effective antibacterial scaffold.

3.7.3. *In vivo experiment*

To assess the wound healing potential of hydrogels, full thickness skin defects were created in SD rats. Subsequently, hydrogel precursor solutions were injected and irradiated by UV light (Fig. S9). Images were taken on week 1, week 2 and week 3 to assess the healing process (Fig. 6A). The results showed that the wound area diminished with time. On week 3, the wound treated with DTP0 and DTP4 hydrogels almost healed whereas, a portion of wound remained unhealed for DP and Blank group. Fig. 6B showed that the percentage of wound closure in different groups. The trend of the wound closure went as Blank < DP < DTP0 < DTP4. By the end of week 3, the wound closure ratio for Blank, DP, DTP0 and DTP4 groups were 82.3 %, 91.6 %, 98.2 % and 100 %, respectively. Moreover, the wound treated with DTP4 hydrogel did not show obvious scar during the healing process.

To observe tissue regeneration during the healing process, tissues samples from the wound bed were processed with H&E and Masson's staining. Fig. 6C represents the H&E staining of tissues. All groups depicted the sign of inflammation near epithelium marked with blue arrowhead indicating the wounds were passing through the inflammatory phase. However, wound treated with DTP4 showed a slight inflammation indicating that this group had shifted to the healing phase. The redness around the epithelium was indicative of aggregation of red blood cells and various other clotting factors.

Similarly, neutrophilic infiltration around the skin is also indicative of inflammation. In week 2, staining of all wounds had generally overcome inflammation except the blank where neutrophilic infiltration was still visible. The epithelial layer had formed completely in week 2 for DTP0 and DTP4 groups. Whereas the untreated group could not form the epithelial layer. H&E staining further confirmed the tissue organization and maturation (black dotted box) in DTP4 group. The presence of hair follicles, indicated with a yellow arrowhead, were visible in week 2. Similarly, epithelial layer was also much mature. These signs indicate that DTP4 had a remarkable influence during the regenerative process.

To assess the tissue organization and collagen fibre deposition,

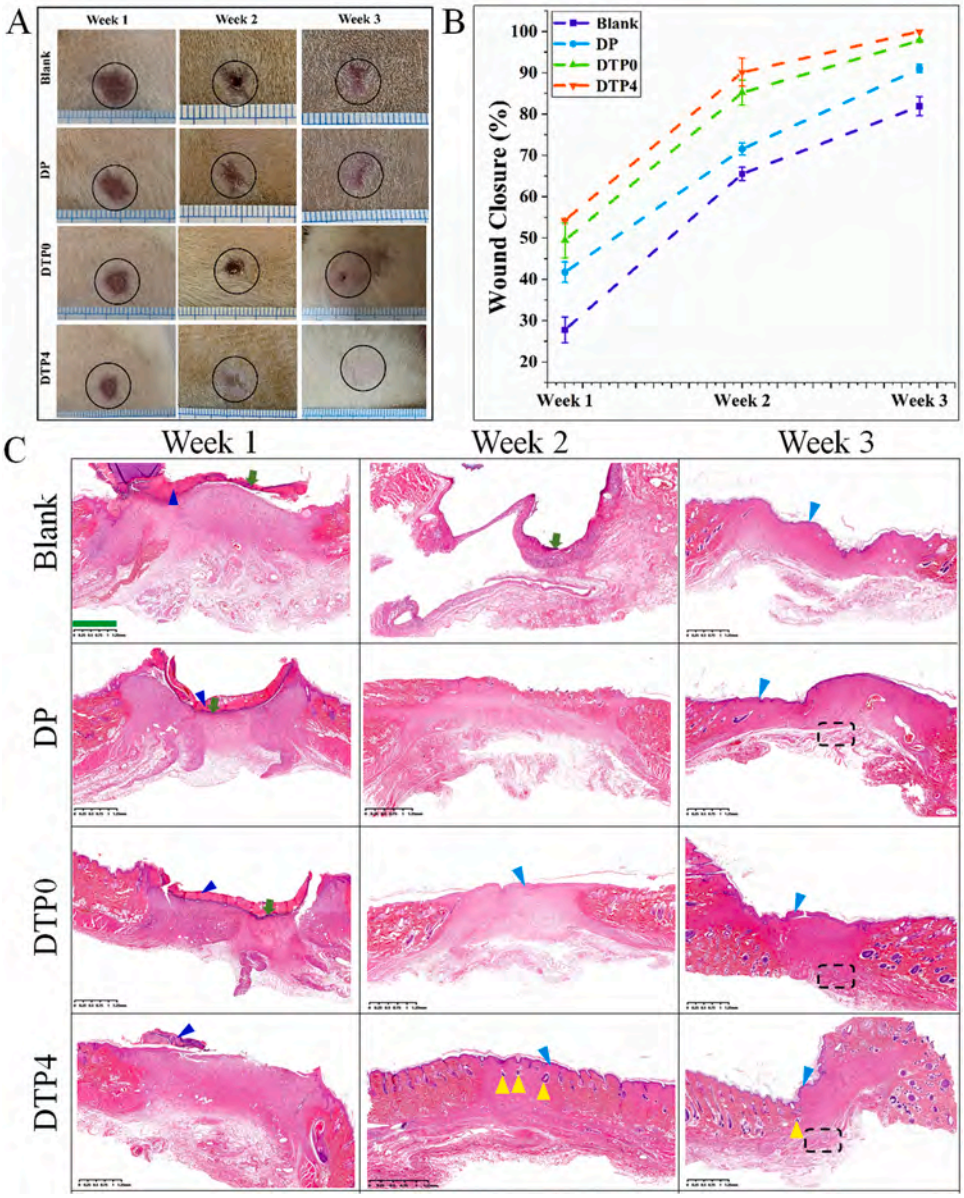

Fig. 6. Representative image of *in vivo* experiment. (A) The progress of wound closure with time, (B) Percentage of wound closure at certain timepoints, (C) H&E staining of wound treated with hydrogels. Epithelization, neutrophilic infiltration and inflamed tissue are represented by the blue arrowhead, green arrow and dark blue arrowhead, respectively. Hair follicles and collagen organization are represented by the yellow arrowhead and black dotted box, respectively. Scale bar is 1.25 mm. Each group tested three independent samples.

Masson's staining was performed (Fig. 7A). The early signs of inflammation in week 1 were observed in all groups (yellow arrow). Blood vessel in wound bed could be observed in groups specially for DTP4 (black arrow). To assess the healing quality, we encircled the newly formed tissues by yellow dotted square. And results showed that tissue organization improved in hydrogels groups, especially for DTP4.

The collagen fibre was highly organized and fibre-like appearance. Similarly, some structures such as sebaceous glands indicated by the yellow circle could be observed in DTP4, further supporting its effect in tissue organization. Moreover, the presence of adipose tissues indicated by green arrow (Fig. 7A DTP4 at week3) indicated tissue differentiation in DTP4. CD31 marker was used to identify the endothelial cells density in newly healed wounds. The immunochemical staining of CD31 showed a clear difference in endothelial cells density at different time-points (Fig. 7B). The red arrow indicated the counter-stained areas to precisely locate the endothelial layer. The positive endothelial cell staining was indicative by blue arrowhead. DTP4 showed a denser distribution of endothelial cells (purple arrowhead). The presence of endothelial cells indicated rich angiogenesis in newly formed tissue, which indicated the better quality of wound healing.

4. Discussion

Wound healing is a complex and multiphasic process that requires an optimum environment [33]. Many innovative wound dressings have been designed to accelerate the healing process by imparting an active role in various phases of healing [3]. An ideal wound dressing should have attributes such as close mimicry with native tissues to provide growth signals, suitable mechanical strength and biodegradability, antimicrobial properties, biocompatibility and moist environment around wound [34,35].

The dECM contains collagen, glycosaminoglycans, laminins and growth factors that are same compositions as the natural extracellular matrix [8,12,36]. Besides, dECM can significantly improve cell adhesion. Chitosan is a widely used biomaterial [37,38]. It promotes the activity of macrophages, the migration of neutrophils and regulates the expression of growth factors [39–41]. Studies showed that chitosan scaffolds could generate synergistic effect on wound healing [42–44]. Recent studies showed that the hydrophilic nanofiber can provide structural similarity and cellular ingrowth [23,25]. Furthermore, the angiogenesis, macrophage polarization and wound healing were also

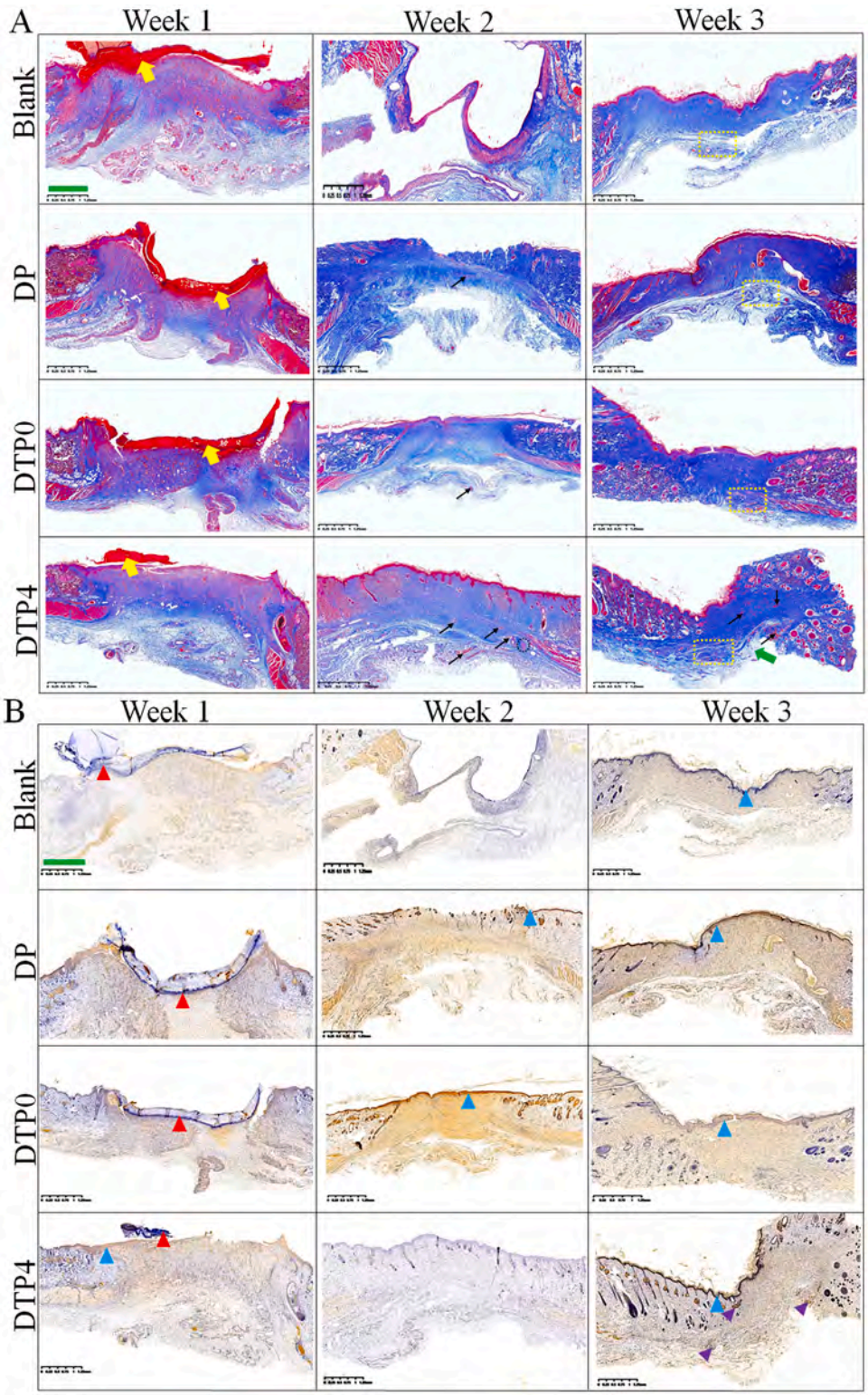

Fig. 7. Histopathological studies of newly formed tissue at various time-points. (A) Masson's staining of tissues treated with hydrogels. Inflamed tissues (yellow arrow), blood vessels (black arrow), sebaceous glands (black dotted circle, DTP4 at week 2), adipose tissue (green arrow), organization of collagen (yellow dotted square) are represented by different signs, respectively. (B) CD31 staining showing the endothelial cells. CD31 counterstaining, positive staining and positive epithelial staining are represented as red, purple and blue arrowhead, respectively. Scale bar is 1.25 mm.

enhanced.

ddECM is a decellularized product of dermal matrix, sharing same chemical composition. After decellularization, cellular components are removed. Histological examination confirmed the similar structure of ddECM and fresh dermis (Fig. 2C-F). The residual DNA and virus in decellularized tissues has been the main obstacle to functioning as a scaffold. Therefore, triton X-100 and peracetic acid are used. The result in Fig. 2B showed the concentration of residual DNA, which is lower than that in previous report [16].

ddECMMA hydrogels are thermally responding hydrogels, also exhibiting optical crosslinking capabilities [45]. As previously reported [10,17], the methacrylation of ddECM prevent self-assembly and could not form nanostructure. No nanostructure of ddECMMA was observed in DP hydrogel (Fig. 3C). Meanwhile, PCLPBA could be seen in DTP0 and DTP4 and it resulted in the enhanced mechanical properties and porosity. The graft of BA onto PCLP may create potential covalent

crosslinking [23].

Wound dressing requires adequate mechanical strength. Results show that Young's modulus and compression strength were significantly higher in DTP4 than others (Figs. 4B, 4C). This can be attributed to delicate fibre structures and TCS. The densely packed fibrillar network poses an excellent resistance to an axial tensile force [30]. A similar trend was observed in swelling ratio (Fig. 4D).

Biodegradability is necessary for scaffold to avoid secondary damage to newly formed tissues. Since we selected naturally degradable constituents, DP and DTP0 almost degraded completely within 24 h. DTP4 remained 58 % while PEG remained over 97 % (Fig. 4E). The reason could be the permittance of enzyme-containing liquid inside hydrogel. We also find that TCS slowed down the hydrogel degradation process due to dense network inside.

An intact skin serves as a structure that resists microbial invasion and infection. However, the wound always remains at high risk of developing infection due to damage to the barrier. Conventional approach is to load antibacterial agents in the scaffold. However, the abuse of antibiotics may pose the risk of bacterial resistance and associated cytotoxicity [46]. We made our scaffold antimicrobial by using natural chitosan derivative, which could encapsulate bacteria and subsequently lead to their death [28,47]. *E. coli* and *S. aureus,* representing Gram-negative and Gram-positive respectively, were tested (Fig. 5D). Our results, obtained through the colony counting method, indicated that only DTP4 hydrogel could resist colony formation (Fig. S8). Its antibacterial potential can be correlated to TCS. Chitosan is capable of disrupting the bacterial wall resulting in the leakage of cytoplasmic contents [48]. The antibacterial potential can be greatly improved by thioglycolic acid modification [28]. Our results support this because no colony was observed in DTP4 group.

Thioglycolic acid is a widely used reducing agent and can be oxidized easily [49]. The graft of thioglycolic acid makes TCS capable of free radical scavenging by forming intermolecular and intramolecular disulfide bonds [21,50]. Result showed that DTP4 has good antioxidant activity (Fig. 5C). which can reduce the overproduction of reactive oxygen species in wound area [51].

Since wound dressing come in close contact with body tissues, its biocompatibility is a pre-required attribute. We culture NIH 3T3 on hydrogel scaffold. The result showed that all hydrogels were non cytotoxic as the number of viable cells was present in high number (Fig. 5A). Live & dead staining also indicated that viable cells were orienting into tissue-like structures, especially in DTP0 and DTP4 groups (Fig. 5B). This can be attributed to nanofiber, which facilitated cell orientation and proliferation. Besides, chitosan and its derivatives have extensively reported for good effect on wound healing and angiogenesis [3,37,52]. Howling et al. reported that chitosan might interact with growth factors in the serum and potentiated their effect, which stimulates fibroblast proliferation [53]. Okamoto et al. reported that chitosan and their oligomers/monomers enhanced the migration of fibroblasts (3T3) and vascular endothelial cells (HUVEC) *in vitro* [54]. The DTP4 is effective in cell proliferation than due to TCS probably.

Wound healing requires a coherent and ordered role of multiple cells, growth factors, signaling molecules and supply of nutrients [55]. ECM provides the platform for cellular infiltration and migration. Since wounds create damage to the ECM network, the re-establishment of ECM is a prerequisite for the smooth regeneration of tissues. We fabricated the hydrogel with natural ddECM to mimic ECM components. The results demonstrated that DTP4 treated groups exhibited fast wound closure and highly improved tissue organization compared to other counterparts and untreated group (Fig. 6A, 6B). DTP4 in the early phase of wound healing remained prominent because all the wounds except DTP4 showed a clear sign of inflammation near the epithelium (Fig. 6C). According to a previous study, estrogen could enhance the VEGF production from BMSCs, which contributes to macrophage activation, angiogenesis and wound healing [56]. While testosterone decreases growth factor production in stem cells [57]. In the experiment, female SD rats were chosen, and wound healing was almost finished in 2 weeks for DTP4 group. Therefore, the healing process probably extended in mature male rats, since their estrogen concentration is lower than that of mature female rats [58].

5. Conclusion

In this study, a multifunctional decellularized matrix hydrogel with nanofiber was successfully prepared with excellent antibacterial property and skin regeneration property. The hydrogel possessed excellent antibacterial capacity against both Gram-negative and Gram-positive bacteria owing to the addition of thiolated chitosan (TCS). It is interesting that the addition of methacrylating decellularized dermal extracellular matrix (ddECMMA) and Poly (ethylene glycol) diacrylate (PEGDA) into hydrogel could lead to short gelation time and improved mechanical property. 3-buten-1-amine (BA) modified polycaprolactone nanofiber (PCLPBA) in hydrogel simulated the structure of native extracellular matrix, improved the mechanical strength of hydrogel and cell proliferation. Besides, the similarity of components between ddECMMA and native dermal tissue promoted skin wound healing. The SD rat models showed that DTP4 group could promote wound healing, which has excellent potential in skin tissue regeneration. Therefore, we envisioned that the DTP4 hydrogels possessed great potentials in biomedical applications, especially in skin regeneration. It will be important that future research investigate the potential mechanism of DTP4 hydrogel on wound healing, for example its effect on regulation of caspase 8 in the granular layer, production of pro-inflammatory cytokines and chemokines in wound area.

CRediT authorship contribution statement

Fan Yu: Conceptualization, Methodology, Software, Data curation, Writing- Original draft. **Atta ur Rehman Khan:** Methodology, Software, Validation, Formal analysis, Resources. **Hui Zheng:** Methodology, Validation, Data curation. **Xiaotong Li:** Investigation, Resources. **Mohamed EL-Newehy:** Investigation, Data curation. **Hany EL-Hamshary:** Investigation, Resources. **Yosry Morsi:** Investigation, Resources. **Jun Li:** Supervision, Project administration. **Jinglei Wu:** Supervision, Project administration. **Xiumei Mo:** Supervision, Project administration, Funding acquisition.

Declaration of Competing Interest

The authors declare that they have no known competing financial interests or personal relationships that could have appeared to influence the work reported in this paper.

Data Availability

The authors do not have permission to share data.

Acknowledgement

This research was supported by Science and Technology Commission of Shanghai Municipality, China (No.19441902600, 20S31900900, 20DZ2254900, 20S31901400, 19441901700, 19441901701, 19441901702) and Sino German Science Foundation Research Exchange Center, China (M-0263) and National Natural Science Foundation of China, China (81970091). This project was also supported by Researchers Supporting Project Number (RSP-2021/65), King Saud University, Riyadh, Saudi Arabia, National Advanced Functional Fiber Innovation Center, China (2021-fx020301), International Cooperation of China 2021–2022 and Poland Science and Technology Personnel Exchange Program, China (No.17).

Appendix A. Supporting information

Supplementary data associated with this article can be found in the online version at doi:10.1016/j.colsurfb.2022.112691.

References

[1] L. Ouyang, et al., A generalizable strategy for the 3D bioprinting of hydrogels from nonviscous photo-crosslinkable inks, Adv. Mater. 29 (8) (2017).
[2] J. Qu, et al., Antibacterial adhesive injectable hydrogels with rapid self-healing, extensibility and compressibility as wound dressing for joints skin wound healing, Biomaterials 183 (2018) 185–199.
[3] Y. Yang, et al., Mussel-inspired adhesive antioxidant antibacterial hemostatic composite hydrogel wound dressing via photo-polymerization for infected skin wound healing, Bioact. Mater. 8 (2022) 341–354.
[4] M. Liu, et al., Injectable hydrogels for cartilage and bone tissue engineering, Bone Res 5 (2017) 17014.
[5] D. Zhou, Y. Ito, Visible light-curable polymers for biomedical applications, Sci. China Chem. 57 (4) (2014) 510–521.
[6] A.J. Neumann, T. Quinn, S.J. Bryant, Nondestructive evaluation of a new hydrolytically degradable and photo-clickable PEG hydrogel for cartilage tissue engineering, Acta Biomater. 39 (2016) 1–11.
[7] G. Chen, N. Kawazoe, Y. Ito, Photo-Crosslinkable Hydrogels Tissue Eng. Appl., Photochem. Biomed. Appl. (2018) 277–300.
[8] A. Pacifici, et al., Decellularized hydrogels in bone tissue engineering: a topical review, Int J. Med Sci. 15 (5) (2018) 492–497.
[9] S. Baiguera, et al., Electrospun gelatin scaffolds incorporating rat decellularized brain extracellular matrix for neural tissue engineering, Biomaterials 35 (4) (2014) 1205–1214.
[10] E.C. Beck, et al., Approaching the compressive modulus of articular cartilage with a decellularized cartilage-based hydrogel, Acta Biomater. 38 (2016) 94–105.
[11] H.K. Cheung, et al., Composite hydrogel scaffolds incorporating decellularized adipose tissue for soft tissue engineering with adipose-derived stem cells, Biomaterials 35 (6) (2014) 1914–1923.
[12] A. Damania, et al., Decellularized liver matrix-modified cryogel scaffolds as potential hepatocyte carriers in bioartificial liver support systems and implantable liver constructs, ACS Appl. Mater. Interfaces 10 (1) (2017) 114–126.
[13] Y. Zhou, et al., Photopolymerized maleilated chitosan/methacrylated silk fibroin micro/nanocomposite hydrogels as potential scaffolds for cartilage tissue engineering, Int J. Biol. Macromol. 108 (2018) 383–390.
[14] M.J. Robertson, et al., Optimizing recellularization of whole decellularized heart extracellular matrix, PloS One 9 (2) (2014), e90406.
[15] B.B. Rothrauff, et al., Efficacy of thermoresponsive, photocrosslinkable hydrogels derived from decellularized tendon and cartilage extracellular matrix for cartilage tissue engineering, J. Tissue Eng. Regen. Med 12 (1) (2018) e159–e170.
[16] J. Kshersagar, et al., Decellularized amnion scaffold with activated PRP: a new paradigm dressing material for burn wound healing, Cell Tissue Bank 19 (3) (2018) 423–436.
[17] B.B. Rothrauff, et al., Efficacy of thermoresponsive, photocrosslinkable hydrogels derived from decellularized tendon and cartilage extracellular matrix for cartilage tissue engineering, J. Tissue Eng. Regen. Med. 12 (1) (2018) e159–e170.
[18] M.M. Hassan, Antibacterial and antifungal thioglycolic acid-capped silver nanoparticles and their application on wool fabric as a durable antimicrobial treatment, ChemistrySelect 2 (1) (2017) 504–512.
[19] W. Tang, et al., The cadmium–mercaptoacetic acid complex contributes to the genotoxicity of mercaptoacetic acid-coated CdSe-core quantum dots, Int. J. Nanomed. 7 (2012) 2631.
[20] M. Croce, et al., Synthesis and screening of N-acyl thiolated chitosans for antibacterial applications, Carbohydr. Polym. 151 (2016) 1184–1192.
[21] D. Sakloetsakun, J.M. Hombach, A. Bernkop-Schnürch, In situ gelling properties of chitosan-thioglycolic acid conjugate in the presence of oxidizing agents, Biomaterials 30 (31) (2009) 6151–6157.
[22] A. Bernkop-Schnürch, M. Hornof, D. Guggi, Thiolated chitosans. Eur. J. Pharm. Biopharm.: Off. J. Arb. Fur Pharm. Verfahr. E. V. 57 (1) (2004).
[23] X. Li, et al., Nanofiber-hydrogel composite-mediated angiogenesis for soft tissue reconstruction, Sci. Transl. Med. 11 (490) (2019).
[24] Z. Feng, et al., Bioinspired nanofibrous glycopeptide hydrogel dressing for accelerating wound healing: a cytokine-free, M2–type macrophage polarization approach, Adv. Funct. Mater. 30 (52) (2020), 2006454.
[25] X. Li, et al., The effect of a nanofiber-hydrogel composite on neural tissue repair and regeneration in the contused spinal cord, Biomaterials 245 (2020), 119978.
[26] M.T. Wolf, et al., A hydrogel derived from decellularized dermal extracellular matrix, Biomaterials 33 (29) (2012) 7028–7038.
[27] J. Visser, et al., Crosslinkable hydrogels derived from cartilage, meniscus, and tendon tissue, Tissue Eng. Part A 21 (7–8) (2015) 382.
[28] G. Geisberger, et al., Chitosan-Thioglycolic Acid as a Versatile Antimicrobial Agent, Biomacromolecules 14 (4) (2013) 1010–1017.
[29] X.-F. Sun, et al., Preparation and swelling behavior of pH/temperature responsive semi-IPN hydrogel based on carboxymethyl xylan and poly (N-isopropyl acrylamide), Cellulose 26 (3) (2019) 1909–1922.
[30] A.U.R. Khan, et al., , Multifunctional bioactive core-shell electrospun membrane capable to terminate inflammatory cycle and promote angiogenesis in diabetic wound, Bioact. Mater. 6 (9) (2021) p. 2783–2800.
[31] Z. Ganim, et al., Amide I two-dimensional infrared spectroscopy of proteins, Acc. Chem. Res. 41 (3) (2008) 432–441.
[32] M. Fevzioglu, et al., Quantitative approach to study secondary structure of proteins by FT-IR spectroscopy, using a model wheat gluten system, Int. J. Biol. Macromol. 164 (2020) 2753–2760.
[33] Y. Liang, J. He, B. Guo, Functional hydrogels as wound dressing to enhance wound healing, ACS nano 15 (8) (2021) 12687–12722.
[34] M.R. MacEwan, et al., What makes the optimal wound healing material? a review of current science and introduction of a synthetic nanofabricated wound care scaffold, Cureus 9 (10) (2017), e1736.
[35] L. Yildirimer, N.T. Thanh, A.M. Seifalian, Skin regeneration scaffolds: a multimodal bottom-up approach, Trends Biotechnol. 30 (12) (2012) 638–648.
[36] H. Debels, et al., Dermal matrices and bioengineered skin substitutes: a critical review of current options, Plast. Reconstr. Surg. Glob. Open 3 (1) (2015), e284.
[37] B. Kaczmarek, A. Sionkowska, A.M. Osyczka, Scaffolds based on chitosan and collagen with glycosaminoglycans cross-linked by tannic acid, Polym. Test. 65 (2018) 163–168.
[38] S. Kim, et al., Photocrosslinkable chitosan hydrogels functionalized with the RGD peptide and phosphoserine to enhance osteogenesis, J. Mater. Chem. B 4 (31) (2016) 5289–5298.
[39] M. Lu, et al., Fabrication of photo-crosslinkable glycol chitosan hydrogel as a tissue adhesive, Carbohydr. Polym. 181 (2018) 668–674.
[40] R. Jayakumar, et al., Biomaterials based on chitin and chitosan in wound dressing applications, Biotechnol. Adv. 29 (3) (2011) 322–337.
[41] C. Chen, et al., Multifunctional Chitosan Inverse Opal Particles for Wound Healing, ACS nano 12 (10) (2018) 10493–10500.
[42] J.-Y. Shin, S.-J. Jeong, W.-K. Lee, Fabrication of porous scaffold by ternary combination of chitosan, gelatin, and calcium phosphate for tissue engineering, J. Ind. Eng. Chem. 80 (2019) 862–869.
[43] B.K. Gu, et al., Gelatin blending and sonication of chitosan nanofiber mats produce synergistic effects on hemostatic functions, Int. J. Biol. Macromol. 82 (2016) 89–96.
[44] L. Nie, et al., Development of chitosan/gelatin hydrogels incorporation of biphasic calcium phosphate nanoparticles for bone tissue engineering, J. Biomater. Sci., Polym. Ed. 30 (17) (2019) 1636–1657.
[45] I.D. Gaudet, D.I. Shreiber, Characterization of methacrylated type-I collagen as a dynamic, photoactive hydrogel, Biointerphases 7 (1–4) (2012) 25.
[46] R.J. Fair, Y. Tor, Antibiotics and bacterial resistance in the 21st century. Perspectives in medicinal chemistry 6 (2014) 25–64.
[47] H. Li, et al., Injectable, self-healing, antibacterial, and hemostatic N, O-carboxymethyl chitosan/oxidized chondroitin sulfate composite hydrogel for wound dressing, Mater. Sci. Eng.: C. 118 (2021), 111324.
[48] D. Raafat, H.-G. Sahl, Chitosan and its antimicrobial potential–a critical literature survey. Microbial biotechnology 2 (2) (2009) 186–201.
[49] T. Shi, J. Berglund, L.I. Elding, Kinetics and mechanism for reduction of trans-dichlorotetracyanoplatinate (IV) by thioglycolic acid, L-cysteine, DL-penicillamine, and glutathione in aqueous solution, Inorg. Chem. 35 (12) (1996) 3498–3503.
[50] I. Gout, Coenzyme A: a protective thiol in bacterial antioxidant defence, Biochem. Soc. Trans. 47 (1) (2019) 469–476.
[51] A.U.R. Khan, et al., Physico-chemical and biological evaluation of PLCL/SF nanofibers loaded with oregano essential oil, Pharmaceutics 11 (8) (2019).
[52] T.H. Kim, Y. Jung, S.H. Kim, Nanofibrous electrospun heart decellularized extracellular matrix-based hybrid scaffold as wound dressing for reducing scarring in wound healing, Tissue Eng. Part A 24 (9–10) (2018) 830–848.
[53] G.I. Howling, et al., The effect of chitin and chitosan on the proliferation of human skin fibroblasts and keratinocytes in vitro, Biomaterials 22 (22) (2001) 2959–2966.
[54] Y. Okamoto, et al., Effects of chitin/chitosan and their oligomers/monomers on migrations of fibroblasts and vascular endothelium, Biomaterials 23 (9) (2002) 1975–1979.
[55] I. Pastar, et al., Epithelialization in Wound Healing: a comprehensive review, Adv. Wound Care 3 (7) (2014) 445–464.
[56] C.E. Routley, G.S. Ashcroft, Effect of estrogen and progesterone on macrophage activation during wound healing, Wound Repair Regen.: Off. Publ. Wound Heal. Soc. Eur. Tissue Repair Soc. 17 (1) (2009) 42–50.
[57] R. Ray, et al., Deleterious effects of endogenous and exogenous testosterone on mesenchymal stem cell VEGF production, Am. J. Physiol. Regul., Integr. Comp. Physiol. 294 (5) (2008) R1498–R1503.
[58] J.O. Jansson, S. Edén, O. Isaksson, Sexual dimorphism in the control of growth hormone secretion, Endocr. Rev. 6 (2) (1985) 128–150.